J. Biochem. **134**, 101–110 (2003)
DOI: 10.1093/jb/mvg117

Contribution of Conserved Amino Acids at the Dimeric Interface to the Conformational Stability and the Structural Integrity of the Active Site in Ketosteroid Isomerase from *Pseudomonas putida* Biotype B

Gyu Hyun Nam[1,3], Do-Hyung Kim[*,1,3], Nam-Chul Ha[2,3], Do Soo Jang[1,3], Young Sung Yun[1,3], Bee Hak Hong[1,3], Byung-Ha Oh[2,3] and Kwan Yong Choi[†,1,3]

[1]National Research Laboratory of Protein Folding and Engineering; [2]National CRI Center for Biomolecular Recognition; and [3]Division of Molecular and Life Sciences, Pohang University of Science and Technology, Pohang, 790-784, South Korea

Received March 12, 2003; accepted May 2, 2003

Ketosteroid isomerase (KSI) from *Pseudomonas putida* biotype B is a homodimeric enzyme catalyzing an allylic isomerization of Δ^5-3-ketosteroids at a rate of the diffusion-controlled limit. The dimeric interactions mediated by Arg72, Glu118, and Asn120, which are conserved in the homologous KSIs, have been characterized in an effort to investigate the roles of the conserved interface residues in stability, function and structure of the enzyme. The interface residues were replaced with alanine to generate the interface mutants R72A, E118A, N120A and E118A/N120A. Equilibrium unfolding analysis revealed that the $\Delta G_U^{H_2O}$ values for the R72A, E118A, N120A, and E118A/N120A mutants were decreased by about 3.8, 3.9, 7.8, and 9.5 kcal/mol, respectively, relative to that of the wild-type enzyme. The interface mutations not only decreased the k_{cat}/K_M value by about 8- to 96-fold, but also increased the K_D value for *d*-equilenin, a reaction intermediate analogue, by about 7- to 17.5-fold. The crystal structure of R72A determined at 2.5 Å resolution and the fluorescence spectra of all the mutants indicated that the interface mutations altered the active-site geometry and resulted in the decreases of the conformational stability as well as the catalytic activity of KSI. Taken together, our results strongly suggest that the conserved interface residues contribute to stabilization and structural integrity of the active site in the dimeric KSI.

Key words: conserved interface residues, dimeric enzyme, dimeric interactions, ketosteroid isomerase, site-directed mutagenesis.

Abbreviations: KSI, ketosteroid isomerase; *E. coli, Escherichia coli*; SDS–PAGE, sodium dodecyl sulfate-polyacrylamide gel electrophoresis; pSK(–), pBluescript SK(–); 5-AND, 5-androstene-3,17-dione; EDTA, ethylenediaminetetraacetic acid; DTT, dithiothreitol; CD, circular dichroism; rms, root mean square; $\Delta G_U^{H_2O}$, free-energy change for unfolding in the absence of urea at 25°C; *B* factors, average temperature factors; TIM, triose phosphate isomerase.

Ketosteroid isomerase (KSI)[1] is a homodimeric enzyme catalyzing an allylic isomerization of a variety of Δ^5-3-ketosteroids to Δ^4-3-ketosteroids by an intramolecular transfer of C-4β proton to C-6 of the steroid (Scheme 1) (*1*). KSI is one of the most proficient enzymes exhibiting a reaction rate of the diffusion-controlled limit (*2*). The enzyme has been extensively investigated as a prototype to understand the catalytic mechanism of the allylic rearrangement (*3–9*). Structural analyses of two homologous KSI enzymes from different bacterial species, *Pseudomonas putida* biotype B and *Comamonas testosteroni*, by X-ray crystallography (*8–10*) and NMR spectroscopy (*11*, *12*) have significantly contributed to the understanding of the mechanism for efficient catalysis of KSI.

In spite of extensive studies on the reaction mechanism of KSI (*3–9*), few studies have been carried out on the role of the dimeric interactions in stabilizing the active site of KSI. Many proteins form dimers even though each monomer contains the complete active site for their enzymatic functions. In the dimeric triose phosphate isomerase, an interface mutation, H47N, resulted in formation of the monomer, which was virtually inactive and energetically very unstable (*13*). In some cases, interface mutations affected the protein stability or activity of the dimeric state rather than induced the formation of the monomeric state. In case of the dimeric manganese superoxide dismutase from *E. coli*, Y174F mutation reduced its activity by about 2-fold and resulted in structural changes at the metal-binding site, even though Tyr174 is located at the dimeric interface and quite remote from the active-site metal center (*14*). Similar examples can also be found for oligomeric proteins. For instance, P105G mutation, which disrupts subunit contacts in hexameric nucleoside diphosphate kinase from

[*]Present address: Whitehead Institute for Biomedical Research, Nine Cambridge, Cambridge, MA 02142, USA.
[†]To whom correspondence should be addressed. Tel: +82-54-279-2295, Fax: +82-54-279-2199, E-mail : kchoi@postech.ac.kr

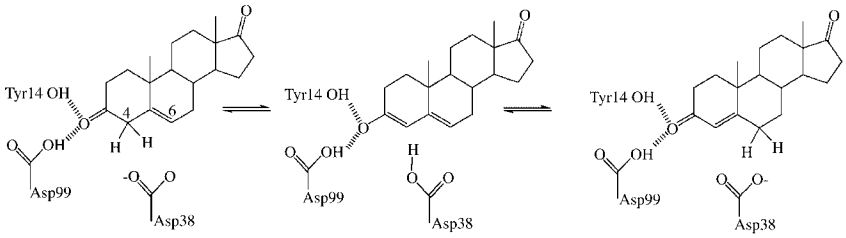

Scheme 1. **General catalytic mechanism of KSI.** KSI catalyzes isomerization reaction; proton at C4 of the steroid substrate, 5-androstene-3,17-dione, is transferred to the catalytic base Asp38 of the enzyme to generate the dienolate intermediate, which is stabilized by the hydrogen bonds of both Tyr14 and Asp99, and then the same proton is transferred to C6 to generate the product, 4-androstene-3,17-dione.

Dictyostelium discoideum, decreased the enzymatic activity by 2-fold at 37°C, and reduced the thermal transition midpoint from 61.8 to 37.8°C (*15*). The above examples of oligomeric proteins imply that the intersubunit interactions contribute to the conformational stability and the structural integrity required for their optimal biological functions.

KSI is a homodimer in which each monomer has 125 or 131 amino acids for *C. testosteroni* KSI or *P. putida* KSI, respectively (*16–18*). Because the KSI interface is symmetric, the same residues can be found symmetrically on opposite sides of the dimeric interface consisting of a narrow and long path of β-sheets (Fig. 1). Each monomer contains one active site consisting of the residues emanating from the same monomer. At the center of the interfacial β-sheets, hydrophobic residues account for most of the dimeric contacts; but at the edge of the interface, three residues with a polar side chain can be found: Arg72, Glu118, and Asn120 (the residues of the *P. putida* KSI are numbered from 1 to 131 for monomer 1 and from 201 to 331 for monomer 2 of the dimer according to those of the *C. testosteroni* KSI (Fig. 1). Although two KSI enzymes have only 34% identity in their amino acid sequences, their dimeric interaction modes and the residues that participate in hydrogen bonding across the interface are well conserved in both KSIs (*8–12*), implying potential contributions of the conserved interface residues to the conformational stability or the catalytic activity of KSI.

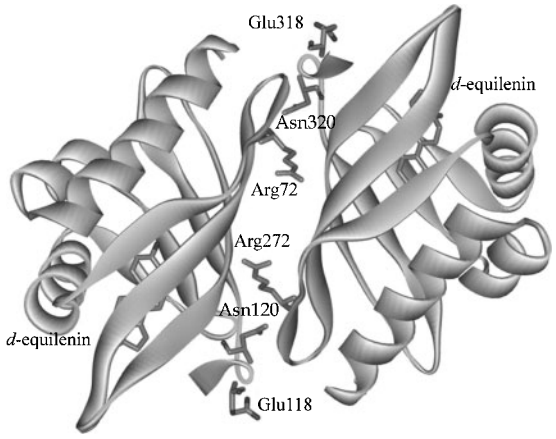

Fig. 1. **Ribbon diagram for the three-dimensional structure of *P. putida* KSI in complex with *d*-equilenin, a reaction intermediate analogue.** The three interface residues, Arg72, Glu118 and Asn120, as well as *d*-equilenin are shown in a ball-and-stick model. The KSI structure was generated by the Molscript program (*19*). The side chains of three conserved residues at the dimeric interface are oriented away from the active site, while the steroid is bound to the hydrophobic active site of KSI.

To assess the roles of the dimeric interactions mediated by the conserved interface residues, Arg72, Glu118, and Asn120 were each replaced with alanine, and the effects of these mutations on the stability, activity and structure of KSI were investigated. The interface mutations decreased the conformational stability as well as the catalytic activity while altering the active-site geometry of the dimeric KSI. Our results provided an insight into the significance of the dimeric interactions for the conformational stability as well as the structural integrity of the active site in the dimeric KSI.

MATERIALS AND METHODS

Reagents and Experimental Procedures—Ultrapure urea was purchased from Sigma. T4 DNA ligase and restriction enzymes were obtained from Roche Molecular Biochemicals. Oligonucleotides were obtained from Bioneer, Korea. Radiochemicals for sequencing were purchased from Amersham Pharmacia Biotech. 5-androstene-3,17-dione (5-AND) was purchased from Stealoid. 5-AND exhibited a single spot on the thin layer chromatographic analysis and its molecular weight was confirmed by mass spectrometry as described previously (*20*). All other chemicals were molecular-biology grade from Sigma. The protein concentration was determined by use of the difference extinction coefficient (2,330 $M^{-1}cm^{-1}$ per tyrosine residue) between tyrosinate and tyrosine at 295 nm as described previously (*21*). The accuracy of the protein concentration was confirmed by the quantitative analysis of the protein bands on SDS–PAGE using an imaging densitometer (Bio-Rad, GS-700).

Site-Directed Mutagenesis—Arg72, Glu118, and Asn120 were replaced with alanine by oligonucleotide-directed mutagenesis to make R72A, E118A, N120A, and E118A/N120A according to the procedure as described previously (*22*); single-stranded and uracil-containing template DNA complementary to the coding strand of the isomerase gene was obtained from pSW2 (*23*), a recombinant pBluescript SK(–) plasmid (Stratagene) containing the *P. putida* KSI gene, which had been introduced into *E. coli* RZ1032 after infection with the helper phage M13K07 (Amersham Pharmacia Biotech). Three oligonucleotides, 5′-CTG ACC GGG CCG GTA GCG GCT AGC CAT AAC GGC TGC-3′ for R72A, 5′-AA GCC TAC TGG AGC GCT GTC AAC CTC AGC GTG C-3′ for E118A, and 5′-C TAC TGG AGC GAG GTC GCG CTC AGC GTG CGC GAG C-3′ for N120A, were synthesized and used as a primer for the respective mutagenesis; the underlined nucleotides represent those changed for mutations. The double mutant E118A/N120A was prepared similarly by

mutagenesis using the single-stranded DNA of N120A as a template and 5′-AA GCC TAC TGG AGC GCT GTC GCG CTC AGC GTG C-3′ as a primer. The entire genes encoding the interface mutant KSIs were sequenced to confirm the desired mutations. The mutated gene subcloned into pSK(–) was digested with *Eco*RI and *Hin*dIII to isolate the inserted DNA fragment containing the entire KSI gene and then ligated into the *Eco*RI and *Hin*dIII sites of pKK223-3 (Amersham Pharmacia Biotech) to construct the recombinant plasmid for expression.

Expression and Purification of KSIs—Each mutant KSI was overexpressed as a soluble form in *E. coil* BL21(DE3) and bound specifically to the deoxycholate affinity resin. The bound proteins were eluted from the affinity resin and loaded onto a gel-filtration chromatographic column to purify the mutant KSIs, similarly to the purification of the wild-type enzyme (*18*). The mutant enzymes exhibited single protein bands of identical size corresponding to a molecular mass of about 14 kDa for the monomer upon SDS-PAGE (data not shown).

Solvent-accessible Surface Area—Solvent-accessible surface area was calculated from the atomic coordinates obtained by X-ray crystallography (*8*) utilizing a software program (Molecular Simulations, Quanta version 2.0) according to the procedures described previously (*24*). The probe radius for the calculation was 1.4 Å.

Fluorescence Spectroscopy—Fluorescence measurement was carried out by use of a spectrofluorometer (Shimadzu, RF-5000) equipped with a thermostatically-controlled cell holder. KSI was incubated at a concentration of 15 μM in a buffer containing 25 mM sodium phosphate, pH 7.0, 0.5 mM ethylenediaminetetraacetic acid (EDTA) and 1 mM dithiothreitol (DTT). Emission spectra were recorded between 300 and 400 nm after the KSI sample had been excited at 280 or 295 nm at 25°C.

Circular Dichroism Spectroscopy—Circular dichroism (CD) spectroscopic analyses were performed with a spectropolarimeter (Jasco, 715) equipped with a Peltier type temperature controller (Jasco, PTC-348WI). A cuvette with a path length of 2 mm was used for all the CD spectral measurements. KSI was preincubated at a concentration of 15 μM in a buffer containing 25 mM sodium phosphate, pH 7.0, 0.5 mM EDTA, and 1 mM DTT. The CD spectra were obtained with a scan speed of 10 nm/min and a bandwidth of 2 nm. Scans were collected at 1 nm intervals and accumulated three times at 25°C. Each spectrum was corrected by subtracting the spectrum of the buffer and smoothened utilizing a program provided by the manufacturer of the spectropolarimeter.

Equilibrium Unfolding—Solutions of 15 μM wild-type and mutant enzymes were prepared in a buffer containing 25 mM sodium phosphate, pH 7.0, 0.5 mM EDTA, and 1 mM DTT with various urea concentrations from 0 to 8 M. After incubation at 25°C for longer than 48 h, the fluorescence intensity at 320 nm, the wavelength at the maximum fluorescence intensity, and the molar ellipticity at 222 nm were measured at each urea concentration. The free-energy change (ΔG_U) for denaturation was determined according to a two-state model for denaturation utilizing the following equations (*25*):

$$F_U = (E_N - E)/(E_N - E_U) \quad (1)$$

$$K_U = 2P_T[F_U^2/(1 - FU)] \quad (2)$$

$$\Delta G_U = RT\ln(K_U) = \Delta G_U^{H_2O} - m\cdot[\text{urea}] \quad (3)$$

where F_U is the fraction of unfolded protein, E is the fluorescence intensity at 320 nm, the wavelength at the maximum fluorescence intensity, or the molar ellipticity at the respective urea concentration, E_N and E_U are the observed values for the native and unfolded states, respectively, and P_T is the total protein concentration. The $\Delta G_U^{H_2O}$ value is the free-energy change in the absence of urea, and m represents a measure of ΔG_U dependence on urea concentration. The data from a urea denaturation curve were fitted to Eq. 4 according to the procedures described previously (*26*) by a nonlinear least-square method utilizing a graphics program (Abelbeck Software, Kaleidagraph version 2.6).

$$E = E_N - (E_N - E_U)\exp[(m\cdot[\text{urea}] - \Delta G_U^{H_2O})/RT]\cdot \{\{1 + 8P_T/\exp[(m\cdot[\text{urea}] - \Delta G_U^{H_2O})/RT]\}^{1/2} - 1\}/4P_T \quad (4)$$

The differences in free-energy change for unfolding, $\Delta\Delta G_U$, between the wild-type and mutant enzymes were determined from the following equation:

$$\Delta\Delta G_U = \Delta G_U \cdot \Delta G_U^m \quad (5)$$

where ΔG_U is the free-energy change for unfolding of the wild-type enzyme and ΔG_U^m that of the respective mutant enzymes.

Determination of Enzymatic Activity—The catalytic activities of the wild-type and mutant KSIs were determined spectrophotometrically with a Cary 3E Spectrophotometer using 5-AND as a substrate according to the procedure described previously (*18*). The reaction was carried out at 25°C in the buffer containing 34 mM potassium phosphate, pH 7.0, and 2.5 mM EDTA with the respective substrate concentrations: 12, 35, 58, 82, and 116 μM. Kinetic parameters, k_{cat} and K_M, were determined utilizing the Lineweaver-Burk reciprocal plot. Mean values (± standard deviation) from three independent determinations were obtained for the comparison of kinetic parameters.

Determination of K_D for Equilenin—The dissociation constant, K_D, for equilenin was determined by the fluorescence quenching method as described previously (*27*). The fluorescence measurement was carried out at 25°C with a spectrofluorometer (Shimazu, RF-5000) in a buffer solution containing 10 mM potassium phosphate, pH 7.0, and 5% methanol. The fluorescence intensity of equilenin at 364 nm was obtained and used to calculate the K_D value for equilenin after the excitation at 335 nm for various enzyme concentrations.

Crystallization and Structure Determination of R72A—Crystals of the mutant protein were grown from a solution containing 2.0 M ammonium acetate and 0.1 M sodium acetate at pH 4.6 by the hanging-drop vapor-diffusion method at 22°C as described previously (*8*). Diffraction data were obtained on a DIP2020 area detector with graphite-monochromated Cu Kα X-rays which were generated by a rotating anode generator (MacScience, M18XHF) operated at 90 mA and 50 kV at room temperature. Data reduction, merging and scaling were carried

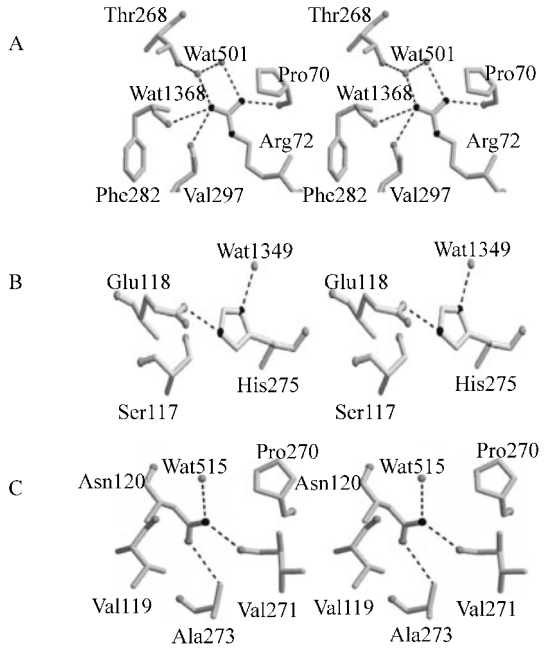

Fig. 2. **Stereoview of the hydrogen-bond interactions mediated by the conserved interface residues of the dimeric KSI.** (A) The guanidine group of Arg72 interacts with Pro70, Phe282, Val297, Wat501, and Wat1368 via hydrogen bonds. (B) The carboxyl group of Glu118 forms the hydrogen bond with the imidazole ring of His275. (C) The carbonyl and amide groups of Asn120 participate in hydrogen bonding with the backbones of Val271 and Ala273, respectively. The oxygen and nitrogen atoms are denoted by gray and black balls, respectively. The figure was drawn using the Molscript program (*19*).

out with the programs DENZO and SCALEPACK as described previously (*28*). The crystal structure of R72A was determined utilizing the atomic coordinates of the wild-type KSI (Brookhaven Protein Data Bank, code 1OPY) and the XPLOR software as described previously (*29*).

RESULTS

Structural Aspects of the Hydrogen Bonds Mediated by Arg72, Glu118, and Asn120 at the Dimeric Interface of KSI—Based on the three-dimensional structure of *P. putida* KSI (*8*), Arg72, Glu118, and Asn120 were found to be located at the dimeric interface and to participate mainly in hydrogen bonding between two monomers. The side chain of Arg72 located in the loop linking β-strands B3 and B4 is mostly buried with a solvent-accessible surface area of about 4 Å^2. Nγ1 in the side chain of Arg72 is hydrogen-bonded with both Wat501 and the carbonyl group of Pro70, while Nγ2 forms a hydrogen-bond network with the carbonyl groups of both Phe282 and Val297 and Wat1368, which also forms a hydrogen bond with the side chain of Thr268 (Fig. 2A, Table 1). The side chain of Glu118 located at the edge of the interface β-strand B6 has a solvent-accessible surface area of 34 Å^2, suggesting that it is relatively well exposed to solvent. The carboxyl group of the side chain interacts with the Nε2 in the imidazole ring of His275 on the β-strand B4, which is in turn linked to Wat1349 by a hydrogen bond

Table 1. **Distances of hydrogen bonds mediated by Arg72, Glu118 and Asn120 at the dimeric interface of *P. putida* KSI[a].**

Amino acid	Atoms	Partner atoms	Distance (Å)
Arg72			
	Nγ1	Pro70 O	3.7
	Nγ1	Wat501 O	3.0
	Nγ2	Phe282 O	3.7
	Nγ2	Val297 O	3.3
	Nγ2	Wat1368 O	3.7
Glu118			
	Oε1	His275 Nε2	2.9
	Oε2	His275 Nε2	3.2
Asn120			
	Nδ2	Val271 O	3.0
	Nδ2	Wat515 O	3.2
	Oδ1	Ala273 N	3.4

[a]The distances are based on the crystal structure of *P. putida* KSI (*8*).

with a distance of ca. 2.75 Å (Fig. 2B). The side chain of Asn120 located on the β-strand B7 acts as a bridge between the amide backbone of Ala273 and the carboxyl backbone of Val271 (Fig. 2C), and its solvent-accessible surface area is about 7 Å^2, indicating that it is partially exposed to solvent.

Fluorescence and Circular Dichroism Spectra of the Wild-type and Mutant Enzymes—The fluorescence spectra of the wild-type and interface mutants were obtained after excitation at 280 nm. The maximum fluorescence intensity was increased for all the mutant enzymes and much more significantly for the N120A and E118A/N120A mutants compared with that of the wild-type enzyme (Fig. 3). The wavelength at the maximum fluorescence intensity was observed at 340 nm for the wild-type enzyme, while it was red-shifted to 341.5, 342, 344, and 344.5 nm for the R72A, E118A, N120A, and E118A/N120A mutants, respectively. This result reveals that the environments of Trp116 and the tyrosine triad, Tyr14-Tyr55-Tyr30, near the active site might become more exposed to the aqueous environment (*30*) by the mutations. The fluorescence spectra obtained after excitation at 295 nm exhibited similar patterns (data not shown) to

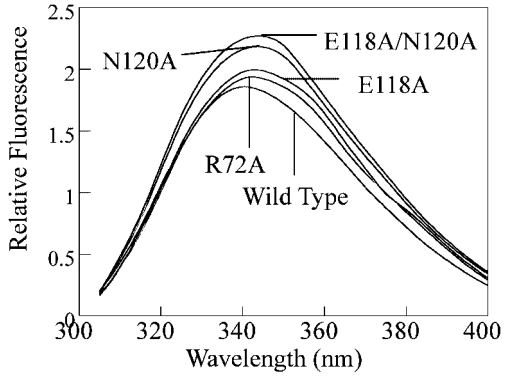

Fig. 3. **Fluorescence emission spectra of the wild-type and mutant KSIs after excitation at 280 nm.** The measurement was carried out with 15 μM concentration of each enzyme in the buffer containing 25 mM potassium phosphate, 0.5 mM EDTA and 1 mM DTT at pH 7.0. The emission spectra were obtained between 300 and 400 nm after the KSI sample was excited at 280 nm at 25°C

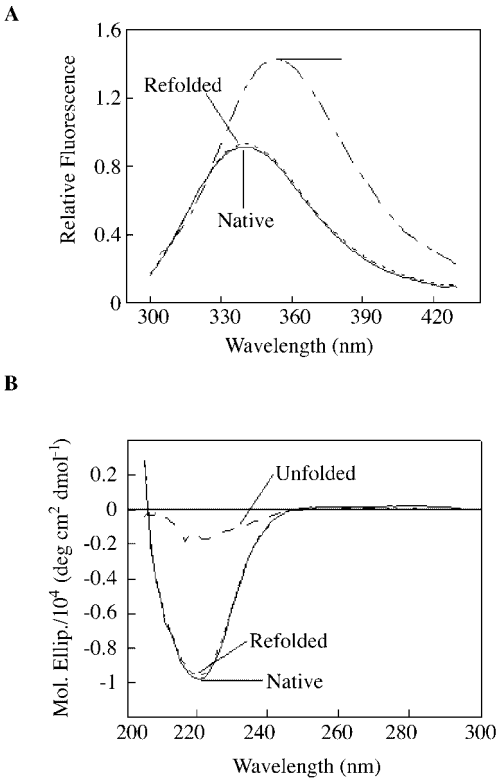

Fig. 4. **Reversibility of folding for the interface mutants in secondary and tertiary structures.** Representative (A) fluorescence and (B) CD spectra of native, unfolded, and refolded KSI protein are displayed for comparison. The fluorescence spectra of the proteins were obtained after excitation at 280 nm. The protein concentration was 15 μM. The unfolded protein was prepared by incubating the protein at 8 M urea for longer time than 48 h. The refolded protein was prepared by diluting the unfolded protein to 0.2 M urea and incubating for longer time than 48 h. The experiments were performed at 25°C in the buffer containing 20 mM potassium phosphate, pH 7.0, 0.5 mM EDTA and 1 mM DTT. All the interface mutants displayed the similar fluorescence and CD spectra at native, unfolded and refolded states.

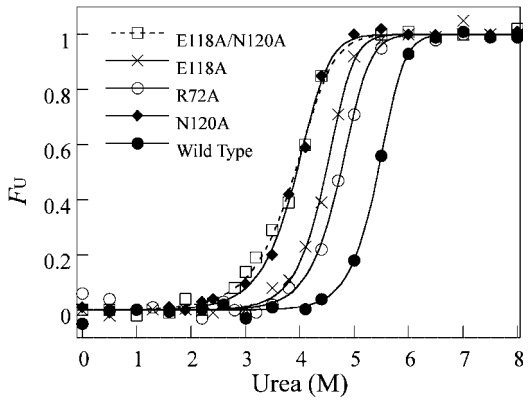

Fig. 5. **Unfolding equilibrium transition curves of the wild-type and interface mutant enzymes.** The fraction of unfolded protein at each urea concentration was calculated from the fluorescence intensity at 320 nm, the wavelength at the maximum fluorescence intensity, and the CD signal at 222 nm after correction for the pre- and post-transition baselines. The data were obtained with 15 μM of each protein in the buffer containing 25 mM potassium phosphate, 0.5 mM EDTA and 1 mM DTT at pH 7.0 with various urea concentrations. The data points were fitted to equation (4) to obtain the transition curve, which enabled us to determine $\Delta G_U^{H_2O}$ and m in Table 2.

those obtained after excitation at 280 nm, implying that the environment of Trp116 might be perturbed by the mutations. The fluorescence spectra of N120A and E118A/N120A were changed more significantly than those of R72A and E118A. Meanwhile, far-UV CD spectra exhibited only marginal differences between the wild-type and mutant KSIs, while the spectral regions around 197 and 222 nm were slightly altered by the mutations (data not shown), indicating that the mutations do not significantly affect the overall secondary structure of the native enzyme.

Reversibility of Folding for the Interface Mutants—The reversible folding of the KSI mutants was analyzed by comparing fluorescence and CD spectra of the protein being refolded with those of the native protein, while the unfolded protein in 8 M urea was diluted successively to lower urea concentrations under reducing conditions. All the interface mutants also exhibited the original activities after refolding. Their wavelengths at the maximum fluorescence intensity were red-shifted to 355 nm (Fig. 4A) and their negative molar elllipticities were significantly decreased in the unfolded state (Fig. 4B), similarly to the wild-type enzyme (*31*). The fluorescence intensities of all the mutant enzymes were decreased in the range of 327–400 nm and increased in the range of 300–327 nm as the urea concentration was increased. The good agreement between the fluorescence or CD spectra of the native and the refolded proteins indicates that the overall secondary and tertiary structures were recovered after refolding.

Mutational Effects on the Conformational Stability—Equilibrium unfolding experiments were carried out to assess the mutational effects on the conformational stability of KSI. The unfolding transition curve was normalized by assuming that the fluorescence intensity at 320 nm, the wavelength at the maximum fluorescence intensity of KSI, and the molar ellipticity for the native and unfolded states can be extrapolated linearly into the transition zone (Fig. 5). There is no indication of any folding intermediates in the unfolding transition curve. The transition curves were almost coincident between CD and fluorescence measurements. These results suggest that folding of KSI mutants can be explained by a two-state model at equilibrium (*31*, *32*).

By applying a two-state model, such values as $\Delta G_U^{H_2O}$, m, $[\text{urea}]_{50\%}$ and $\Delta\Delta G_U$ for the wild-type and mutant enzymes were obtained according to Eqs. 3–5 (Table 2). The $\Delta G_U^{H_2O}$ values of the single-point mutants R72A, E118A, and N120A were decreased by about 3.8, 3.9 and 7.8 kcal/mol, respectively, compared with that of the wild-type enzyme, suggesting that the dimeric interactions mediated by the conserved residues are important for the conformational stability of KSI. Especially, the mutational effects of N120A and E118A/N120A were significant. N120A was unfolded at a lower urea concentration than R72A and E118A. The $\Delta G_U^{H_2O}$ value of E118A/N120A was lower than that of the wild-type enzyme by about 9.5 kcal/mol. All the mutant enzymes exhibited

Table 2. **Changes in the free energies of unfolding of the wild-type and mutant KSIs determined by reversible denaturation with urea[a].**

Enzyme	$\Delta G_U^{H_2O}$ [b] (kcal/mol)	m[c] (kcal/mol M)	$[urea]_{50\%}$[d] (M)	$\Delta\Delta G_U$[e] (kcal/mol)
Wild Type	24.3 ± 0.5	3.39 ± 0.07	5.22 ± 0.10	–
R72A	20.5 ± 0.7	3.09 ± 0.11	4.74 ± 0.16	3.8
E118A	20.4 ± 0.4	3.25 ± 0.06	4.46 ± 0.09	3.9
N120A	16.5 ± 0.5	2.72 ± 0.08	3.95 ± 0.12	7.8
E118A/N120A	14.8 ± 0.4	2.30 ± 0.06	3.89 ± 0.11	9.5

[a]Measurements were performed at 25°C and pH 7.0. Values were obtained by fitting the data in Fig. 5 to Eq. 4. [b]$\Delta G_U^{H_2O}$ was determined by extrapolation of the data to urea concentration at 0 M upon denaturation. [c]m is the slope of the linear denaturation plot, $d\Delta G_U/d[urea]$. [d]$[urea]_{50\%}$ is the concentration of urea at which 50% of the protein is unfolded. [e]Values obtained from Eq. 5.

Table 3. **Kinetic parameters of the wild-type and mutant enzymes[a].**

Enzyme	k_{cat} (s^{-1})	K_M (μM)	k_{cat}/K_M (M^{-1} s^{-1})	Relative[b] k_{cat}	Relative[c] K_M	Relative[d] k_{cat}/K_M
Wild Type[e]	21200 ± 810	49.9 ± 1.3	$(4.3 \pm 0.16) \times 10^8$	1.00	1.00	1.00
R72A	4870 ± 67	0.1 ± 1.2	$(5.4 \pm 0.08) \times 10^7$	0.23	1.81	0.13
E118A	6920 ± 74	173 ± 1.9	$(4.0 \pm 0.04) \times 10^7$	0.33	3.48	0.09
N120A	3710 ± 61	258 ± 4.2	$(1.4 \pm 0.02) \times 10^7$	0.17	5.16	0.03
E118A/N120A	1180 ± 34	261 ± 7.5	$(4.5 \pm 0.12) \times 10^6$	0.06	5.23	0.01

[a]The assays were performed in a buffer containing 34 mM potassium phosphate and 2.5 mM EDTA at pH 7.0. The kinetic parameters were obtained from three independent measurements. [b,c,d]Values relative to those of the wild-type enzyme. [e]Values from Kim *et al.* (*27*).

smaller m values, indicating that they might be unfolded less cooperatively than the wild-type enzyme.

Mutational Effects on Catalytic Efficiency and Equilenin Binding—To investigate the effect of the hydrogen bonds mediated by the three interface residues on the catalytic activity, k_{cat} and K_M of the interface mutants were determined using a steroid substrate, 5-AND. The k_{cat} values of the R72A, E118A ,and N120A mutants were moderately decreased by about 4.4-, 3.0-, and 5.9-fold, and their K_M values were increased by *ca.* 1.8-, 3.5-, and 5.2-fold, respectively, relative to that of the wild-type enzyme (Table 3). Even though the mutational effects on the respective kinetic parameters were moderate, those on the k_{cat}/K_M value, representing the specificity for the substrate at low substrate concentration, became much more synergistic. The k_{cat}/K_M values were decreased by about 8- to 31-fold for single-point mutants. Most notably, E118A/N120A had a 96-fold smaller k_{cat}/K_M value than the wild-type enzyme.

The K_D value for *d*-equilenin, a reaction intermediate analogue, was assessed by measuring the extent of quenching for the fluorescence of *d*-equilenin upon binding the enzymes. Relative to the K_D value of the wild-type enzyme, which was reported to be *ca.* 1.9 μM (*27*), those of the mutant enzymes were increased by about 7.2-, 6.6-, and 7.7-fold for the R72A, E118A, and N120A mutants, respectively, and substantially by about 17.5-fold for the E118A/N120A mutant (Table 4).

Crystal Structure of R72A—To investigate the structural changes between the wild-type and interface mutants, crystallization of the mutant enzymes was attempted. Crystals of only R72A could be successfully obtained. The crystal structure of R72A was determined at 2.5 Å resolution. It belongs to the space group *C*2221 with cell dimensions of a = 36.37 Å, b = 74.44 Å, and c = 96.06 Å, which are the same as those of the wild-type crystal (*8*). The parameters of the crystallographic data and refinement are summarized in Table 5. The electron density for the mutated residue was well defined, and the positions of the residues, Pro70, Phe282, and Val297, that form hydrogen bonds with Arg72 in the wild-type KSI were marginally changed (Fig. 6). Within the limit of the coordinate error with 0.23 Å, which was estimated from a *Luzzati* plot (*33*), no major conformational

Table 4. **Dissociation constants, K_D, on binding of *d*-equilenin for the wild-type and mutant enzymes[a].**

Enzyme	K_D (μM)[b]
	d-equilenin
Wild Type	1.90 ± 0.10[c]
R72A	13.6 ± 0.15
E118A	12.5 ± 0.13
N120A	14.6 ± 0.17
E118A/N120A	33.3 ± 0.25

[a]K_D for d-equilenin was determined by measuring the fluorescence change of equilenin upon protein binding. The experiments were carried out in the buffer containing 10 mM potassium phosphate and 5% methanol, pH 7.2. [b]The average value ± standard deviation from three independent measurements are shown. [c]The value from Kim *et al.* (*27*).

Table 5. **Crystallographic data and refinement statistics for R72A.**

Resolution (Å)	2.5
R_{sym} (%)	9.2
Data completeness, $F > 1\sigma$ (%)	95.1
$R_{standard}$ (%)	19.2
R_{free} (%)	27.1
Number of atoms	**951**
Water molecules	26
Average *B* factor	**29.22**
rmsd bond length (Å)	0.014
rmsd bond angles (deg)	1.666
Ramachandran plot (%)	
most favored regions	86.3
additional allowed regions	13.7
disallowed regions	0

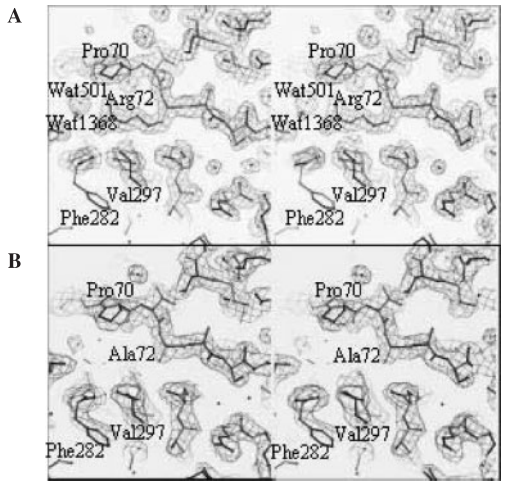

Fig. 6. **Stereodiagram of the local structure surrounding the 72nd residue in the wild-type and R72A mutant enzyme.** A section of the electron density map ($2F_o - F_c$ coefficient, centered at 1.00) of the local structure for the wild type (A) and R72A (B). The structures were displayed using the graphic software O (*19*). The backbones of the wild-type and mutant enzymes are shown as heavy lines.

changes were observed in the crystal structure of R72A. To investigate the observed mutational effects on activity, the residues located near the active site of both the wild-type and R72A enzymes were superimposed, and their rms differences are shown in Table 6. While no significant conformational changes were observed in the crystal structure of R72A, Leu59, Val63, and Met86, which were found not only to interact with *d*-equilenin, but also to sustain the hydrophobic active site of KSI (Fig. 7), exhibited relatively significant values of the local rms difference (Table 6). Temperature factors (*B* factors) for Cα carbons of the active-site residues were moderately

Table 6. **Local rms differences between atomic positions of the wild-type and R72A enzymesa.**

Residuesb	Main-chain	All atoms
Y14	0.11	0.15
V18	0.16	0.20
D38	0.15	0.27
F54	0.22	0.37
L59c	1.27	1.10
V63	0.41	0.49
A65	0.13	0.13
P70	0.23	0.33
M80	0.16	0.17
F82	0.27	0.29
M86	0.47	0.71
W88	0.28	0.52
L95	0.30	0.30
V97	0.30	0.31
D99	0.12	0.19
Mean r.m.s (Å)	0.30 ± 0.08	0.22 ± 0.09

[a]The data are based on the crystal structures of the wild-type (*8*) and R72A enzymes. [b]Only residues located in or near the active site are listed. [c]Residues having the bigger rms difference than 0.4 Å are shown in bold letters.

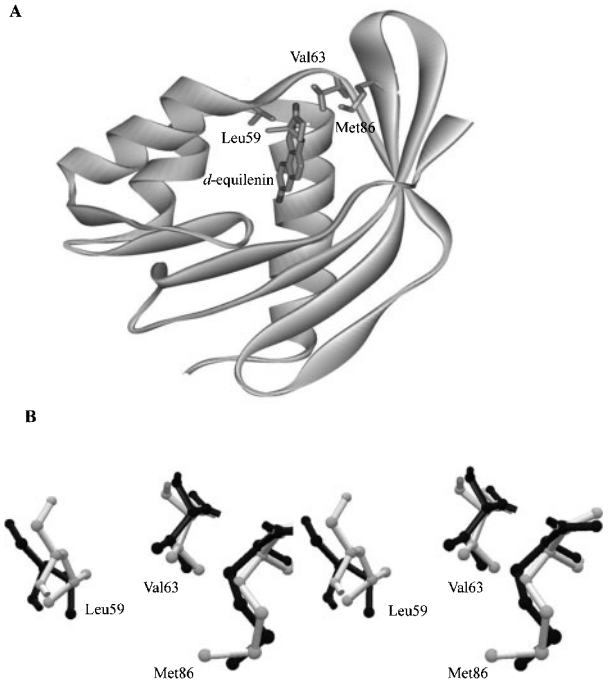

Fig. 7. **Three-dimensional structure of Leu59, Val63, and Met86 in *P. putida* KSI.** (A) Ribbon diagram of three-dimensional structure of Leu59, Val63, and Met86 near the active site. The side chains of Leu59, Val63, and Met86 interact with *d*-equilenin near the active site of KSI. (B) Stereoview of Leu59, Val63, and Met86 in the wild-type and R72A enzymes. Leu59, Val63, and Met86 as well as *d*-equilenin are shown in ball-and-stick model. The equivalent atoms of all the residues in the wild-type (black) and R72A (light gray) enzymes were used for the superposition of the structure. The KSI structure was generated by the Molscript program (*19*).

increased in the crystal structure of R72A relative to those in the crystal structure of the wild-type enzyme (data not shown). In particular, those of three catalytic residues, Tyr14, Asp38, and Asp99, were increased by 7.9, 4.2, and 2.3 Å^2, respectively, even though these residues are deeply located at the active site.

DISCUSSION

The roles of Arg72, Glu118 and Asn120 at the dimeric interface of KSI were investigated by site-directed mutagenesis. Urea-denatured equilibrium unfolding analysis suggested that the dimeric interactions mediated by the conserved interface residues are important for the conformational stability of KSI. Comparison of kinetic parameters of the wild-type and mutant enzymes indicated that the interface residues affected the enzymatic function and the steroid binding of KSI. Analysis of the crystal structure of R72A and the fluorescence spectra of the four interface mutants enabled us to estimate the effects of the interface mutations on the conformational stability and catalytic activity of KSI.

Contribution of the Conserved Interface Residues to the Conformational Stability—The significant decrease of $\Delta G_U^{H_2O}$ in the R72A mutant indicates the importance of Arg72 for conformational stability of KSI. Even though the local structure around Arg72 was not significantly

perturbed, the crystal structure of R72A showed the conformational changes of Leu59, Val63, and Met86 and the increased *B* factors of Tyr14, Asp38, and Asp99 at the active site of KSI. The wavelength at the maximum fluorescence intensity in the R72A mutant was also red-shifted. These observations consistently suggest that Arg72 at the dimeric interface is important for stabilization of the active-site geometry of KSI. The replacement of Glu118 with alanine resulted in the loss of its hydrogen bonding capability to the imidazole ring of His275 from the other monomer. Since Glu118 is well exposed to the solvent and interacts with less neighboring residues than Arg72 and Asn120, the mutational effect on the stability might be less significant than those of the other interface mutants. The mutational effect of N120A on the conformational stability was the most significant among the single-point mutants. The $\Delta G_U^{H_2O}$ value of E118A/N120A was decreased more substantially than those of the single-point mutants. The wavelength at the maximum fluorescence intensity of N120A and E118A/N120A was red-shifted most, indicating that the active sites of these mutant KSIs could be disrupted more significantly than those of the other single-point interface mutants. In addition, N120A and E118A/N120A had relatively smaller *m* values than R72A and E118A. This might be correlated to the difference in accessible surface area upon protein unfolding among the interface mutant enzymes (*34*).

Contribution of the Conserved Interface Residues to Enzymatic Function and Steroid Binding—The replacement of Arg72 with alanine removes the hydrogen bonds formed both with the carbonyl oxygens of Pro70, Phe282 and Val297, and with Wat501 and Wat1368 at the dimeric interface of KSI. Although the side chain of Arg72 is oriented away from the active-site pocket where the steroid binds (Fig. 1), the loss of the dimeric interactions mediated by the side chain of Arg72 affected the binding ability of steroid molecules in the active site as reflected by the decreases of both k_{cat}/K_M and the affinity for equilenin. The crystal structure of R72A showed that the conformational changes of Leu59, Val63, and Met86 at the entry site of the steroid could lead to reduced catalytic efficiency and decreased affinity for the steroid. Even though the rms differences of Tyr14, Asp38, and Asp99 were marginal between the crystal structures of the wild-type and R72A enzymes, the increased *B* factors of three catalytic residues in the R72A structure could imply the alteration of the active-site geometry of KSI, which is consistent with the red-shifted wavelength at the maximum fluorescence intensity in the R72A mutant (Fig. 3). The E118A mutation decreased k_{cat} marginally, but increased K_M significantly relative to that of the R72A mutation. The difference in the mutational effect on k_{cat} and K_M indicates that each mutation might exert its effects differently on binding steroid molecules in KSI. The effect of the N120A mutation on k_{cat} and K_M as well as on the stability was the most substantial among the single-point mutations. The significant red shift of the wavelength at the maximum fluorescence intensity could be due to the conformational changes around Trp116 or the tyrosine triad, Tyr14-Tyr55-Tyr30, near the active site. Thus, the effect of the N120A mutation might originate from the structural perturbation of aromatic residues around the active site of KSI. The extent of decrease in K_D for *d*-equilenin seemed to be correlated with the extent of the decrease in k_{cat}/K_M, implying that the decrease in k_{cat}/K_M might be related to the negative effect of the interface mutations on binding *d*-equilenin.

Relationship between the Conformational Stability and the Enzymatic Function in the Dimeric KSI—Decreases in both stability and activity of KSI were observed upon the interface mutations, suggesting that the stabilization of the dimeric state can be related to the enzymatic function in KSI. The mechanistic basis for the relationship between the conformational stability and the catalytic efficiency of KSI is consistent with the changes of fluorescence spectra induced by the conformational changes around Trp116 or the tyrosine triad, Tyr14-Tyr55-Tyr30, near the active site in the interface mutants. Changes in the wavelength at the maximum fluorescence intensity have been used as an important probe not only to assess conformational stabilities of KSI enzymes, but also to monitor the active-site environment (*25*, *27*, *35*). In our recent studies, the replacement of Trp116 with phenylalanine or alanine reduced the binding affinity for *d*-equilenin and the catalytic activity of KSI (*27*). The elimination of the hydroxyl group or the phenyl ring moiety from the tyrosine triad, Tyr14-Tyr55-Tyr30, near the active site was found to decrease the conformational stability and the catalytic activity of KSI (*25*, *35*). Thus, the interface mutations seem to affect the conformational stability as well as the enzymatic activity, while disrupting the active-site geometry of KSI. Interestingly enough, the extent of red shift of the maximum fluorescence wavelength can also be correlated with the decreases of the catalytic activity and the conformational stability of KSI.

Arg72, Glu118, and Asn120 conserved in both *P. putida* and *C. testosteroni* KSIs were found to be involved in the conformational stability and the enzymatic function while the interface mutations did not disrupt the dimeric KSI completely to generate the unstable monomer. A similar role of the interface residues was also reported in other enzymatic systems. Deletion of the conserved Arg54 at the dimeric interface of κ-bungarotoxin disrupted the structural integrity and led to the formation of an inactive aggregate (*36*). The Y267A mutation at the dimeric interface of transcription factor NFκB p50 destabilized the dimeric protein by 2.0 kcal/mol (*37*). Similar observations were also made in oligomeric proteins as well as dimeric ones. Assembly of tobacco mosaic virus protein into viral coat was found to be triggered by intermolecular hydrogen bonds bridged by water and electrostatic interactions between neighboring subunits (*38*). These results support the significance of the role of the interface residues in oligomeric proteins for the biological function and stability.

In conclusion, the dimeric interactions mediated by Arg72, Glu118, and Asn120 were found not only to contribute to the conformational stability and the structural integrity of KSI, but also to affect the binding interaction with steroid molecules. The structural alteration of the active-site geometry in KSI could provide a physical basis for the correlation between the mutational effects on the conformational stability and the enzymatic function of KSI, even though the crystal structure of R72A and the

fluorescence spectra of the interface mutants provide indicative evidence. Further detailed structural studies of the interface mutant enzymes are necessary to better understand the roles of the interface residues in both the conformational stability and the structural integrity of the dimeric KSI.

This research was supported by grants from the program of the National Research Laboratory sponsored by the Korean Ministry of Science and Technology and from the Korea Science and Engineering Foundation, and G.H. Nam and B.H. Hong in part by the Brain Korea 21 project. The atomic coordinates of R72A were deposited with the entry code of 1C7H at Brookhaven Protein Data Bank.

REFERENCES

1. Ha, N.C., Choi, G., Choi, K.Y., and Oh, B.H. (2001) Structure and enzymology of Δ^5-3-ketosteroid isomerase. *Curr. Opin. Struct. Biol.* **11**, 674–678
2. Kuliopulos, A., Talalay, P., and Mildvan, A.S. (1990) Combined effects of two mutations of catalytic residues on the ketosteroid isomerase reaction, *Biochemistry* **29**, 10271–10280
3. Pollack, R.M., Bantia, S., Bounds, P.L., and Koffman, B.M. (1986) pH dependence of the kinetic parameters for 3-oxo-Δ^5-steroid Isomerase. Substrate catalysis and inhibition by (3S)-spiro[5α-androstane-3, 2-oxiran]-17-one. *Biochemistry* **25**, 1905–1911
4. Xue, L., Kuliopulos, A., Mildvan, A.S., and Talalay, P. (1991) Catalytic mechanism of an active-site mutant (D38N) of Δ^5-3-ketosteroid isomerase: Direct spectroscopic evidence for dienol intermediates. *Biochemistry* **30**, 4991–4997
5. Hawkinson, D.C., Eames, T.C., and Pollack, R.M. (1991) Energetics of 3-oxo-Δ^5-steroid isomerase: source of the catalytic power of the enzyme. *Biochemistry* **30**, 10849–19858
6. Hawkinson, D.C., Pollack, R.M., and Ambulos, N.P.Jr. (1994) Evaluation of the internal equilibrium constant for 3-oxo-Δ^5-steroid isomerase using the D38E and D38N mutants: the energetic basis for catalysis. *Biochemistry* **33**, 12172–12183
7. Choi, G., Ha, N.C., Kim, S.W., Kim, D.H., Park, S., Oh, B.H., and Choi, K.Y. (2000) Asp-99 donates a hydrogen bond not to Tyr-14 but to the steroid directly in the catalytic mechanism of Delta 5-3-ketosteroid isomerase from *Pseudomonas putida* biotype B. *Biochemistry* **39**, 903–909
8. Kim, S.W., Cha, S.S., Cho, H.S., Kim, J.S., Ha, N.C., Cho, M.J., Joo, S.Y., Kim, K.K., Choi, K.Y., and Oh, B.H. (1997) High-resolution crystal structures of Δ^5-3-ketosteroid isomerase with and without a reaction intermediate analogue. *Biochemistry* **36**, 14030–14036
9. Cho, H.S., Choi, G., Choi, K.Y., and Oh, B.H. (1999) Crystal structure of Δ^5-3-ketosteroid isomerase from *Pseudomonas testosteroni* in complex with equilenin settles the correct hydrogen bonding scheme for transition state stabilization. *J. Biol. Chem.* **274**, 32863–32868
10. Cho, H.S., Choi, G., Choi, K.Y., and Oh, B.H. (1998) Crystal structure and enzyme mechanism of Δ5–3-ketosteroid isomerase from *Pseudomonas testosteroni*. *Biochemistry* **37**, 8325–8330
11. Wu, Z.R., Ebrahimian, S., Zawrotny, M.E., Thornbur, L.D., Perez-Alvarado, G.C., Brothers, P., Pollack, R.M., and Summers, M.F. (1997) Solution structure of 3-oxo-Δ^5-steroid isomerase. *Science* **276**, 415–418
12. Massiah, M.A., Abeygunawardana, C., Gittis, A.G., Milvan, A.S. (1998) Solution structure of Δ5–3-ketosteroid isomerase complexed with the steroid 19-nortestosterone hemisuccinate. *Biochemistry* **37**, 14701–14712
13. Borchert, T.V., Zeelen, J.Ph., Scheliebs, W., Callens, M., Minke, W., Jaenicke, R., and Wierenga, R.K. (1995) An interface point-mutation variant of triose phosphate isomerase is compactly folded and monomeric at low protein concentrations. *FEBS Lett.* **367**, 315–318
14. Edwards, R.A., Whittaker, M.M., Whittaker, J.W., Baker, E.N., and Jameson G.B. (2001) Removing a hydrogen bond in the dimer interface of *Escherichia coli* manganese superoxide dismutase alters structures and reactivity. *Biochemistry* **40**, 4622–4632
15. Giartosio, A., Ernet, M., Cervoni, L., Morera, S., Janin, J., Konrad, M., and Lascus, I. (1996) Thermal stability of hexameric and tetrameric nucleoside diphosphate kinases. *J. Biol. Chem.* **271**, 17845–17851
16. Benson, A.M., Jarabak, J., and Talalay, P. (1971) The amino acid sequence of Δ^5–3-ketosteroid isomerase of *Pseudomonas testosteroni*. *J. Biol. Chem.* **246**, 7514–7525
17. Linden, K.G. and Benisek, W.F. (1986) The amino acid sequence of a Δ^5-3-oxosteroid isomerase from *Pseudomonas putida* biotype B. *J. Biol. Chem.* **261**, 6454–6560
18. Kim, S.W., Kim, C.Y., Benisek, W.F., and Choi, K.Y. (1994) Cloning, nucleotide sequence and overexpression of the gene coding for Δ^5-3-ketosteroid isomerase from *Pseudomonas putida* biotype B. *J. Bacteriol.* **176**, 672–6676
19. Choi, G., Ha, N.C., Kim, M.S., Hong, B.H., Oh, B.H., and Choi, K.Y. (2001) Pseudoreversion of the catalytic activity of Y14F by the additional substitution(s) of tyrosine with phenylalanine in the hydrogen bond network of Δ^5-3-ketosteroid isomerase from *Pseudomonas putida* biotype B. *Biochemistry* **40**, 6828–6835
20. Kraulis, P.J. (1991) MOLSCRIPT: a program to produce both detailed and schematic plots of protein structures. *J. Appl. Crystallogr.* **5**, 802–810
21. Copeland, R.A. (1993) *Methods of Protein Analysis: a Practical Guide to Laboratory Protocols*, Chapman and Hall, New York, NY
22. Kunkel, T.A., Roberts, J.D., and Zakour, R.A. (1987) Rapid and efficient site-specific mutagenesis without phenotypic selection. *Methods Enzymol.* **154**, 367–382
23. Kim, S.W. and Choi, K.Y. (1995) Identification of active site residues by site-directed mutagenesis of Δ^5-3-ketosteroid isomerase from *Pseudomonas putida* biotype B. *J. Bacteriol.* **177**, 2602–2605
24. Conolly, M.J. (1983) Analytical molecular surface calculation. *J. Appl. Crystallog.* **16**, 548–558
25. Kim, D.H., Jang, D.S., Nam, G.H., Choi, G., Ha, N.C., Kim, M.S., Oh, B.H., and Choi, K.Y. (2000) Contribution of the hydrogen-bond network involving a tyrosine triad in the active site to the structure and function of a highly proficient ketosteroid isomerase from *Pseudomonas putida* biotype B. *Biochemistry* **39**, 4581–4589
26. Mok, Y.K., de Prat Gay, G.D.P., Butler, P.J., and Bycroft, M. (1996) Equilibrium dissociation and unfolding of the dimeric human papillomavirus strain-16 E2 DNA-binding domain. *Protein Sci.* **5**, 310–319
27. Kim, D.H., Nam, G.H., Jang, D.S., Choi, G., Joo, S., Kim, J.S., Oh, B.H., and Choi, K.Y. (1999) Roles of active site aromatic residues in catalysis by ketosteroid isomerase from *Pseudomonas putida* biotype B. *Biochemistry* **38**, 13810–13819
28. Otwinowski, Z. (1993) In Proceedings of the CCP4 Study Weekend (Sawyer, L. *et al*., eds.) pp. 56–62, SERC Daresbury Laboratory, Warrington, U.K
29. Brünger, A.T. (1992) X-PLOR Version 3.1: a system from X-ray crystallography and NMR. Yale University Press, New Haven, CT
30. Concha, N.O., Head, J.F., Kaetzel, M.A., Dedman, J.R., and Seaton, B.A. (1993) Rat annexin V crystal structure: Ca^{2+}-induced conformational changes. *Science* **261**, 1321–1324
31. Kim, D.H., Nam, G.H., Jang, D.S., Yun, S., Choi, G., Lee, H.C., and Choi, K.Y. (2001) Roles of dimerization in folding and stability of ketosteroid isomerase from *Pseudomonas putida* biotype B. *Protein Sci.* **4**, 741–752
32. Bowie, J.U. and Sauer, R.T. (1989) Equilibrium dissociation and unfolding of the Arc repressor dimer. *Biochemistry* **28**, 7139–7143

33. Luzzati, V. (1952) Traitement statistique des erreurs dans la determination des structures cristallines. *Acta Crystallogr.* **5**, 802–810
34. Myers, J.K., Pacee, C.N., and Scholtz, J.M. (1995) Denaturant *m* values and heat capacity changes: Relation to changes in accessible surface areas of protein unfolding. *Protein Sci.* **4**, 2138–2148
35. Nam, G.H., Jang, D.S., Cha, S.S., Lee, T.H., Kim, D.H., Hong, B.H., Yun, Y.S., Oh, B.H., and Choi, K.Y. (2001) Maintenance of α-helical structures by phenyl rings in the active-site tyrosine triad contributes to catalysis and stability of ketosteroid isomerase from *Pseudomonas putida* biotype B. *Biochemistry* **40**, 13529–13537
36. Grant, G.A., Al-Rabiee, R., Xu, X.L., and Zhang, Y. (1997) Critical interactions at the dimer interface of κ-bungarotoxin, a neuronal nicotinic acetylcholine receptor antagonist. *Biochemistry* **36**, 3353–3358
37. Sengchanthalangsy, L.L., Datta, S., Huang, D.B., Anderson, E., Braswell, E.H., and Ghosh, G. (1999) Characterization of the dimer interface of transcription factor NFκB p50 homodimer. *J. Mol. Biol.* **289**, 1029–1040
38. Perutz, M.F. (1978) Electrostatic effects in proteins. *Science* **201**, 1187–1191